frontiers in Chemistry

ORIGINAL RESEARCH
published: 14 October 2020
doi: 10.3389/fchem.2020.536907

# One Nanoscale Zn(II)-Nd(III) Complex With Schiff Base Ligand: NIR Luminescent Sensing of Anions and Nitro Explosives

*Xia Liu[1], Xiaoping Yang[1]*, Yanan Ma[1], Jieni Liu[1], Dongliang Shi[1], Mengyu Niu[1] and Desmond Schipper[2]*

[1] College of Chemistry and Materials Engineering, Wenzhou University, Wenzhou, China, [2] Department of Chemistry and Biochemistry, The University of Texas at Austin, Austin, TX, United States

One Zn-Nd complex $[Zn_2Nd_4L_2(OAc)_{10}(OH)_2(CH_3OH)_2]$ (**1**) was synthesized from Schiff base ligand bis(3-methoxysalicylidene)ethylene-1,2-phenylenediamine ($H_2L$). **1** shows nanoscale rectangular structure with sizes of about 0.8 × 1.1 × 2.8 nm. **1** exhibits typical near-infrared luminescence of Nd(III) under the excitation of UV-visible light. Further study shows that the complex displays luminescent response behavior to anions and nitro explosives, especially with high sensitivity to $H_2PO_{2-}$ and 2,4,6-trinitrophenol.

**Keywords: lanthanide complex, Schiff base ligand, nanoscale structure, NIR luminescence, luminescent sensing**

OPEN ACCESS

***Edited by:***
*Sidney J. L. Ribeiro, São Paulo State University, Brazil*

***Reviewed by:***
*Marie-Joëlle Menu, Université Toulouse III Paul Sabatier, France*
*Svetlana V. Eliseeva, UPR4301 Centre de Biophysique Moléculaire (CBM), France*

***Correspondence:**
*Xiaoping Yang*
*xpyang@wzu.edu.cn*

***Specialty section:***
*This article was submitted to Inorganic Chemistry, a section of the journal Frontiers in Chemistry*

***Received:*** *02 March 2020*
***Accepted:*** *31 August 2020*
***Published:*** *14 October 2020*

***Citation:***
*Liu X, Yang X, Ma Y, Liu J, Shi D, Niu M and Schipper D (2020) One Nanoscale Zn(II)-Nd(III) Complex With Schiff Base Ligand: NIR Luminescent Sensing of Anions and Nitro Explosives. Front. Chem. 8:536907. doi: 10.3389/fchem.2020.536907*

## INTRODUCTION

Construction of heterometallic d-f nanoclusters has received much interest during recent years because of their unique chemical properties (Peng et al., 2012; Wang et al., 2013; Yang et al., 2014; Andruh, 2015; Wen et al., 2019). Fluorescent response to ions and small molecules has received great attention because of the potential application in many areas such as medicine, biology, and environment (Jankolovits et al., 2011; Sun et al., 2015; Qi et al., 2017). As we know, luminescent lanthanide complexes can show emissions in both visible and near-infrared (NIR) ranges (900–1,600 nm) with sharp emission bands, large Stokes shifts, and long lifetimes (Hu et al., 2017; Ning et al., 2018). At present, many visible luminescent complexes with Tb(III) and Eu(III) ions have been used to detect analytes (Guo et al., 2011; Liu et al., 2013; Shi et al., 2015). However, compared with NIR fluorescent probes based on organic fluorophores (Yuan et al., 2013; Guo et al., 2014), very few NIR luminescent lanthanide complexes with Yb(III), Nd(III), and Er(III) ions have been reported to be used as sensors for the detection (Shi et al., 2019).

Phosphates play a key role in biological energy storage and signal transduction, and nitro explosives such as 2,4,6-trinitrophenol (TNP) are very common ingredients of industrial explosives. Thus, many efforts have been made to design fluorescent sensors for phosphates (Yang et al., 2015; Sedaghat et al., 2019) and nitro explosives (Nagarkar et al., 2014; Liu et al., 2017). Our current research interests are in the design of lanthanide-based complexes with luminescent response to various ions and explosives (Jiang et al., 2018; Shi et al., 2019; Liu et al., 2020). Thus, we report here the synthesis and NIR luminescence properties of a Zn-Nd complex $[Zn_2Nd_4L_2(OAc)_{10}(OH)_2(CH_3OH)_2]$ (**1**) with Schiff base ligand bis(3-methoxysalicylidene)ethylene-1,2-phenylenediamine ($H_2L$, **Scheme 1**).

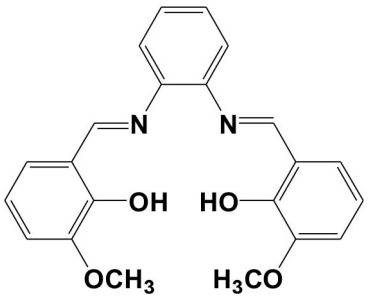


**SCHEME 1 |** Schiff base ligand $H_2L$.

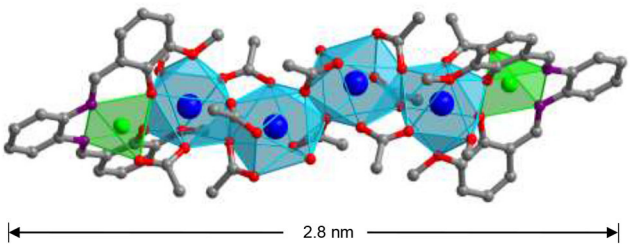


**FIGURE 1 |** The X-ray crystal structure of **1** ($Nd^{3+}$: blue, $Zn^{2+}$: green).

**1** has nanoscale rectangular structure with diameters of 0.8 × 1.1 × 2.8 nm. The complex shows interesting NIR luminescent response behavior to anions and explosives, especially to $H_2PO_2$– and 2,4,6-trinitrophenol (TNP) at ppm level.

## EXPERIMENTAL SECTION

### Preparation of $[Zn_2Nd_4L_2(OAc)_{10}(OH)_2(CH_3OH)_2]$ (1)

$Zn(OAc)_2{\cdot}2H_2O$ (0.30 mmol, 0.0658 g), $NdCl_3{\cdot}6H_2O$ (0.60mmol, 0.2154 g), and $H_2L$ (0.30 mmol, 0.0324 g) were dissolved in 50 mL MeOH at room temperature, and a solution of triethylamine in EtOH (1.0 mol/L, 1 mL) was then added. The mixture was stirred and heated under reflux for 30 min and then filtered. The yellow crystalline product of **1** was obtained by the slow diffusion of diethyl ether into the filtrate at room temperature after 1 month. The crystalline product was collected by filtering and then dried at 120°C in the oven for 2 h. Yield: 0.0981 g (25 %). m. p. > 200°C (dec.). Elemental analysis: found: C, 32.91; H, 4.12; N, 2.50%. Calc. for $C_{72}H_{104}Zn_4Nd_4N_4O_{40}Cl_4$ ($[Zn_2Nd_4L_2(OAc)_{10}(OH)_2(CH_3OH)_2]{\cdot}[ZnCl_2(H_2O)CH_3OH]$): C, 32.68; H, 3.96; N, 2.12%. IR ($CH_3CN$, $cm^{-1}$): 1,703 (s), 1,551 (s), 1,484 (s), 1,289 (s), 1,239 (s), 1,193 (s), 1,072 (m), 963 (s), and 845 (s).

### X-Ray Crystallography

A Smart APEX CCD diffractometer was used to collect the X-ray data of **1** at 190 K. The structure was solved by the direct method (SHELX 97 program) (Sheldrick, 1997). Non-hydrogen atoms were refined anisotropically. Hydrogen atoms were included in the structure factor calculation but not refined. See http://www.rsc.org/suppdata/cc/ for the crystallographic data of **1** in CIF format (CCDC no. 1971956). The selected bond lengths and angles for the structure of **1** are listed in **Supplementary Table 1**.

For **1**: $C_{72}H_{104}Zn_4Nd_4N_4O_{40}Cl_4$, triclinic, space group P-1, $a = 9.6222(19)$, $b = 14.771(3)$, $c = 18.303(4)$ Å, $\alpha = 104.25(3)°$, $\beta = 98.18(3)°$, $\gamma = 103.42(3)°$, $V = 2{,}397.0(8)$ $Å^3$, $Z = 1$, $Dc = 1.833\ g\ cm^{-3}$, $\mu(\text{Mo-K}\alpha) = 3.305\ mm^{-1}$, $F(000) = 1{,}312$, $T = 190$ K. $R_1 = 0.0731$, $wR_2 = 0.1934$, GOF = 1.036.

## RESULTS AND DISCUSSION

### Synthesis and Crystal Structure of the Complex

The Schiff-base ligand $H_2L$ was prepared according to the literature report (Lam et al., 1996; Liu et al., 2020). For the synthesis of d-f complexes, the proportion of raw materials in the reaction may affect the composition of the product. Reaction of $H_2L$ with $Zn(OAc)_2{\cdot}2H_2O$ and $NdCl_3{\cdot}6H_2O$ in a molar ratio of 1:1:2 gave **1**, in which the ratio of $L^{2-}$:$Zn^{2+}$:$Nd^{3+}$ is 1:1:2. The slow diffusion of diethyl ether into the reaction solution led to the formation of yellow crystalline product of **1**. This diffusion way helps to produce pure product of **1**, but results in the low yield (25%), because there are still a large number of product in the mother solution. In the crystalline solid product, zinc chloride ($[ZnCl_2(H_2O)CH_3OH]$) coexists with the complex. The crystal structure of **1** is shown in **Figure 1**. It is centrosymmetric with two equivalent $ZnNd_2L$ moieties linked by two $OAc^-$ anions. The molecular dimensions of **1** are about 0.8 × 1.1 × 2.8 nm. In the $ZnNd_2L$ moiety, $Zn^{2+}$ ion exhibits a square pyramidal geometry, coordinated with the $O_2N_2$ cavity of $L^{2-}$. The coordination number of $Nd^{3+}$ ions is nine, with a single cap square antiprism geometry. The $L^{2-}$ ligand is coordinated with metal ions using two nitrogen and two oxygen atoms. In **1**, the average distance between neighboring $Nd^{3+}$ ions is 4.088 Å. The bond lengths of Zn-N, Zn-O, and Nd-O are 2.036–2.047, 1.994–2.012, and 2.314–2.679 Å, respectively.

Because of the volatilization of solvent molecules in the product, the complex loses about 5% of the weight when heated before 100°C (**Supplementary Figure 2**, thermogravimetric analysis). It is stable until the heating temperature is about 200°C. Molar conductivity study indicates that **1** is neutral in $CH_3CN$, in agreement with its crystal structure. This suggests that **1** remains its unique molecular structure in solution.

### Photophysical Properties and Response to Analytes

The free $H_2L$ shows UV-visible (UV-vis) absorption bands originated from the $\pi - \pi^*$ transition, which are red-shifted in **1** due to the perturbation of metal ions to the transition (**Figure 2**). Metal organometallic chromophores with Zn(II) ion in **1** may efficiently transfer energy to lanthanide ions and sensitize lanthanide luminescence ("antenna effect") (Xu et al., 2010). Thus, excited by ligand-centered absorption bands, **1**

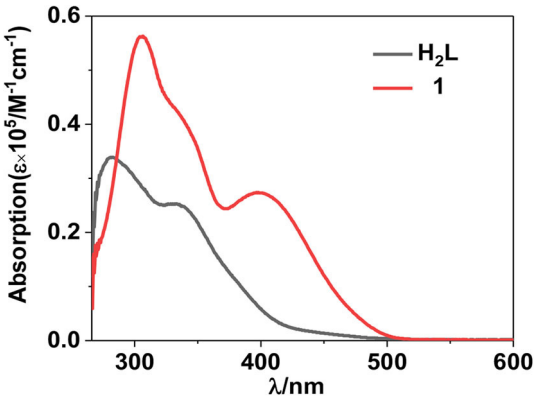


**FIGURE 2 |** UV-visible spectra of the free ligand $H_2L$ and complex **1** at 298 K.

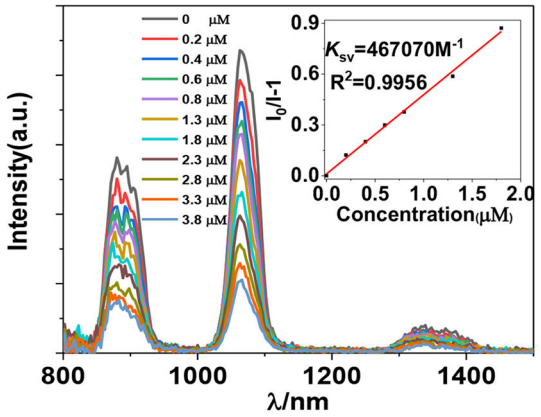


**FIGURE 4 |** Lanthanide luminescent response of **1** (5 μM) to $H_2PO_{2-}$ anion in $CH_3CN$ ($\lambda_{ex}$ = 395 nm).

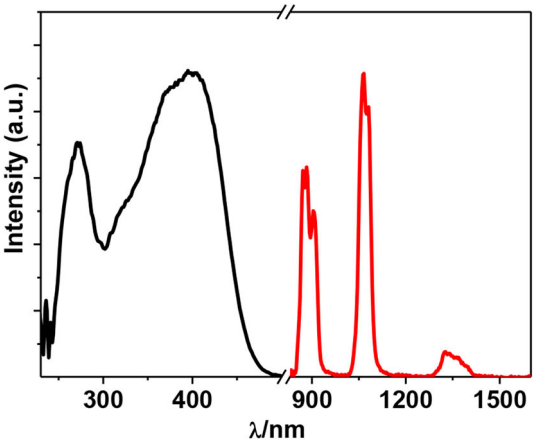


**FIGURE 3 |** Excitation ($\lambda_{em}$ = 1,054 nm) and emission ($\lambda_{ex}$ = 395 nm) spectra of **1** (50 μM) in $CH_3CN$ at 298 K.

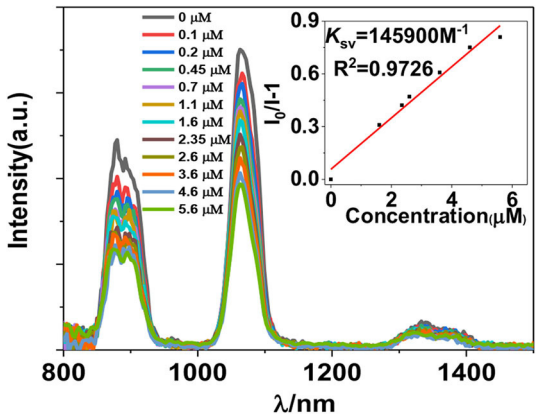


**FIGURE 5 |** Lanthanide luminescent response of **1** (5 μM) to TNP in $CH_3CN$ ($\lambda_{ex}$ = 395 nm).

shows typical NIR luminescence of $Nd^{3+}$ ($^4F_{3/2} \rightarrow {}^4I_{j/2}$ transitions, $j$ = 9, 11, and 13), and the most intense line is at 1,054 nm ($^4F_{3/2} \rightarrow {}^4I_{11/2}$) (**Figure 3**). The complex exhibits broad ligand-centered excitation bands, indicating the ligand-to-metal energy transfer (LMET) in **1**. The NIR emission lifetime ($\tau$) and quantum yield ($\Phi_{em}$) of **1** in $CH_3CN$ are found to be 6.2 μs and 0.8%, respectively.

The luminescent response of **1** toward anions $H_2PO_{2-}$, $F^-$, $CN^-$, $OH^-$, $SO_4^{2-}$, $OAc^-$, $Cl^-$, $Br^-$, $CrO_{4-}$, and $PF_{6-}$, and nitro explosives 2,4,6-trinitrophenol (TNP), 4-nitrochlorobenzene (4-NBC), 2-nitrophenol (2-NP), nitrobenzene (NB), 4-nitrobenzaldehyde (4-NBAP), 4-nitrotoluene (4-NT), 1,3-dinitrobenzene (1,3-DNB), and 4-nitrobenzyl chloride (4-NCB) (**Supplementary Scheme 1**) has been studied in $CH_3CN$. It was found that the addition of all anions and explosives results in a quenching of the lanthanide luminescence (**Supplementary Figures 4, 5**). It is noticeable that the addition of $H_2PO_{2-}$ and TNP causes a more rapid decrease of the luminescence intensities than the addition of other anions and explosives (**Figures 4**, **5**). For example, the emission intensities at 1,054 nm of **1** are decreased more than 50% when the concentrations of added $H_2PO_{2-}$ and TNP are 1.8 and 5.6 μM, respectively, which are much lower than those of other anions and explosives (**Supplementary Figures 4, 5**). These results indicate that **1** shows high selectivity to $H_2PO_{2-}$ and TNP through lanthanide luminescent response.

The addition of anions and explosives with low concentrations, such as <5 μM for $H_2PO_{2-}$ and TNP, results in a linear luminescence quenching response of **1**. Thus, the luminescence quenching efficiencies ($K_{SV}$) of the complex to these analytes can be calculated using Stern–Volmer (S-V) equation $K_{SV} = (I_0/I - 1)/[A]$ (Xiao et al., 2010). As shown in **Figures 6**, **7**, the $K_{SV}$ values of **1** to $H_2PO_{2-}$ and TNP are 4.67 × $10^5$ $M^{-1}$ and 1.46 × $10^5$ $M^{-1}$, respectively, which are much higher than other anions and explosives. The S–V plots of **1** can be explained by static and dynamic quenching models. The static luminescence quenching is generally associated with the formation of ground-state molecular associations upon addition

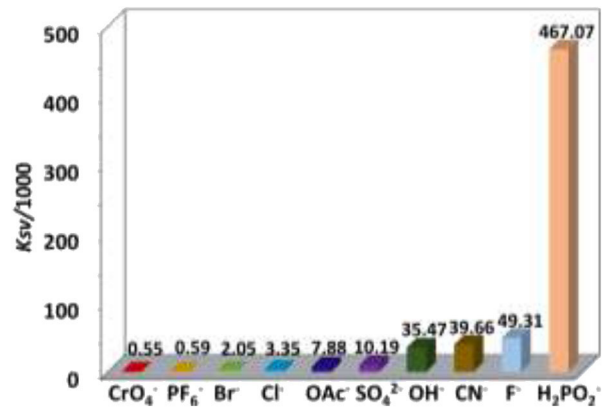


**FIGURE 6 |** NIR emission quenching efficiencies of **1** to anions.

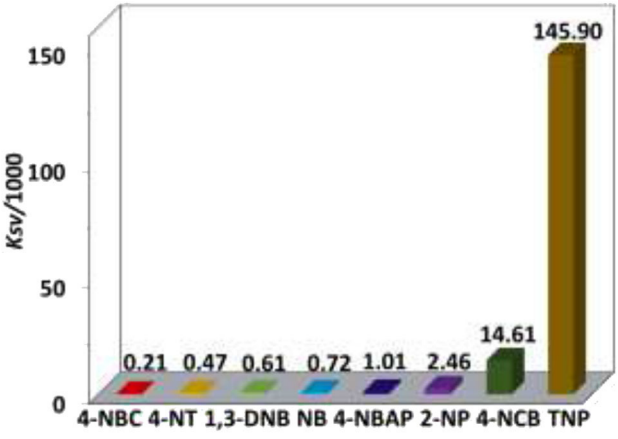


**FIGURE 7 |** NIR emission quenching efficiencies of **1** to explosives.

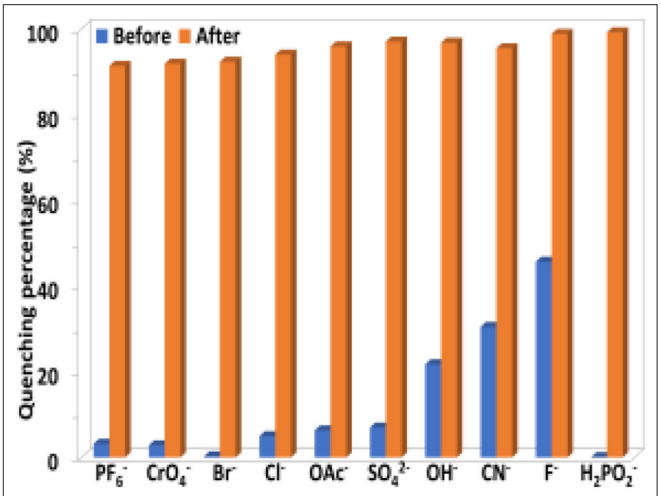


**FIGURE 8 |** The luminescence quenching percentages of **1** (0.5 μM) before and after the addition of $H_2PO_{2-}$ (5 μM) in the presence of other anions (5 μM) in $CH_3CN$.

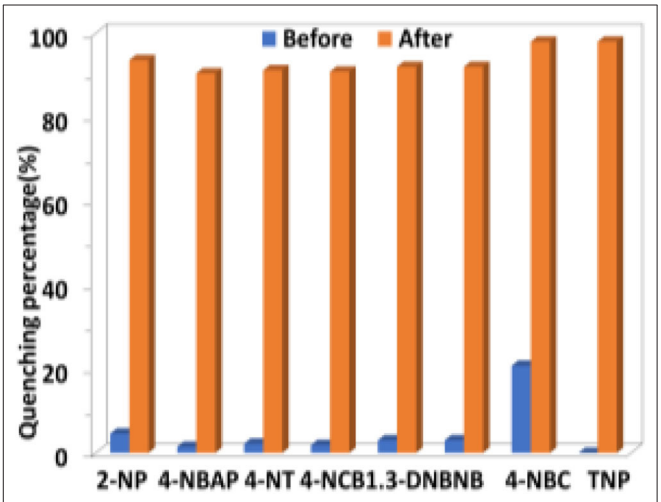


**FIGURE 9 |** The luminescence quenching percentages of **1** (0.5 μM) before and after the addition of TNP (10 μM) in the presence of other explosives (10 μM) in $CH_3CN$.

of the analytes, whereas the dynamic luminescence quenching is under diffusion control, where collisions between analytes and excited fluorophores result in deactivation of the excited states. Basically, the formation of molecular associations in the static quenching model cannot affect the emission lifetimes of fluorophores, however, the collisions in dynamic luminescence quenching may reduce the emission lifetimes. The luminescence lifetimes of **1** are reduced to 4.1 and 5.2 μs with the addition of 1.8 μM of $H_2PO_{2-}$ and 5.6 μM of TNP, respectively, indicating the dominance of dynamic luminescence quenching in **1**.

The selectivity of **1** to $H_2PO_{2-}$ and TNP in the presence of other anions and explosives was investigated. As shown in **Figures 8**, **9**, the existence of another anion and explosive with the same concentration does not affect the high quenching percentage of **1** to $H_2PO_{2-}$ and TNP. These results indicate that **1** shows high selectivity to $H_2PO_{4-}$ and TNP even in the presence of other anions and explosives, respectively.

For luminescent lanthanide complexes, the LMET plays a key role in the intensities of luminescence. The electronic structure and excited state of the Schiff base ligand may be disturbed by the added anions, resulting in the change of the LMET process in **1** (Parker et al., 1998; Parker, 2000). In addition, the possible intermolecular electron transfer from anions to Schiff base ligands may also consume the excitation energy of lanthanide ions and in turn decreases the luminescence of **1** (Guha and Saha, 2010). The intermolecular interaction between the added anions and **1** is crucial to the lanthanide luminescent response. The interaction between $H_2PO_{2-}$ anion and **1** was studied by UV-vis spectral titration (Liu et al., 2017). The red-shift of the absorption bands of **1** indicates the formation of interaction between the added $H_2PO_{2-}$ anion and **1** (**Figure 10**). It is noticeable that the addition of $H_2PO_{2-}$ anion decreases the absorption of **1** at the excitation wavelength ($\lambda_{ex}$ = 395 nm),

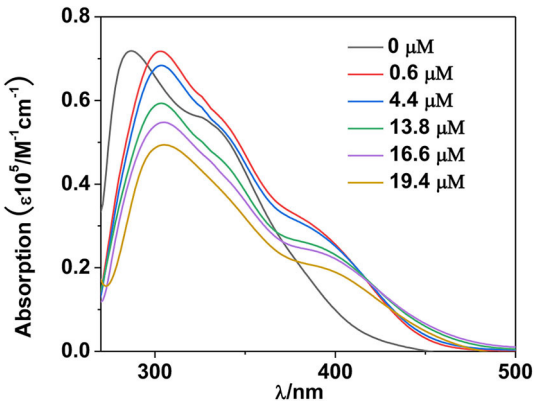


**FIGURE 10 |** UV-visible spectra of **1** with the addition of $H_2PO_{2-}$ anion at 298 K.

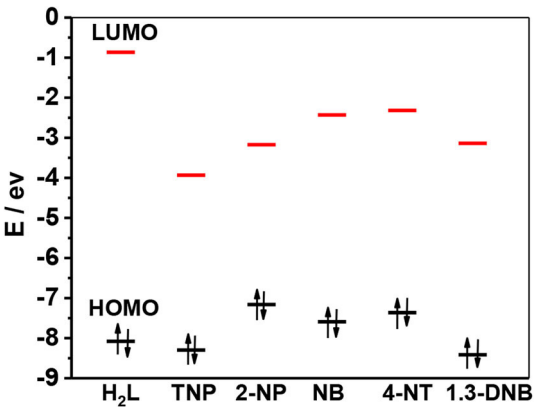


**SCHEME 2 |** HOMO and LUMO energy levels for the free $H_2L$ and selected explosives.

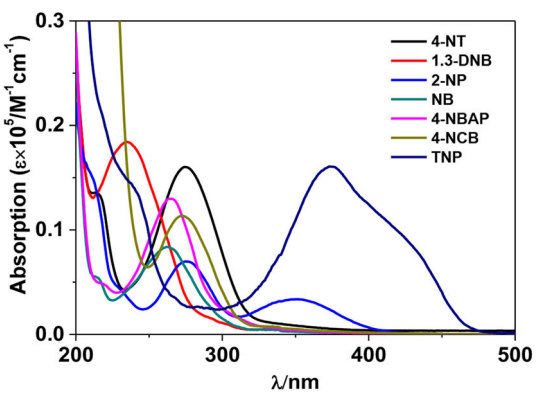


**FIGURE 11 |** UV-vis absorption spectra of explosives in $CH_3CN$.

which is not advantageous for the Schiff base ligand to absorb light energy and further decreases the lanthanide luminescence (Feng et al., 2019).

Usually, the luminescence quenching of lanthanide complexes arisen by the addition of nitro explosives can be explained by photoinduced electron transfer mechanism (Li et al., 2013; Nagarkar et al., 2013; Qin et al., 2015). According to the literature (Xie et al., 2016), the approximate LUMO energy level of $H_2L$ in **1** is shown in **Scheme 2**, which is higher than those of explosives. Thus, the excited electrons of the Schiff base ligand can transfer to the LUMO orbitals of the explosives. TNP has the lowest LUMO energy level among the explosives, which helps in the electron transfer process. Meanwhile, the UV-vis spectra exhibit that TNP has the highest molar absorption at $\lambda_{ex}$ = 395 nm, compared with other explosives (**Figure 11**). This indicates that TNP may compete with **1** for the excitation energy, resulting in the further decrease of lanthanide luminescence.

## CONCLUSIONS

In brief, one Zn-Nd complex **1** with dimensions of 0.8 × 1.1 × 2.8 nm was constructed from Schiff base ligand $H_2L$. The structure of **1** is determined by X-ray crystallography. **1** shows the typical emission of Nd(III) under the excitation of UV-vis light. The addition of anions and nitro explosives leads to a quenching of the luminescence, with high sensitivity of **1** to $H_2PO_{2-}$ and TNP. UV-vis spectral titration confirms the formation of interaction between $H_2PO_{2-}$ anion and **1**, and the addition of $H_2PO_{2-}$ anion decreases the absorption of **1** at the excitation wavelength of lanthanide luminescence. TNP has the lowest LUMO energy level among the added explosives. The addition of TNP results in the competition of excitation energy between the explosive and **1**. Further investigations focused on the construction and luminescent response properties of lanthanide-based complexes are in progress.

## DATA AVAILABILITY STATEMENT

The datasets generated for this study can be found in the Cambridge Crystallographic Data Centre (CCDC number: 1971956).

## AUTHOR CONTRIBUTIONS

XY conceived and designed the experiments. XL, YM, JL, and DS performed the experiments. MN and DS analyzed the data. All authors contributed to the article and approved the submitted version.

## FUNDING

This work was supported by the National Natural Science Foundation of China (No. 21771141).

## SUPPLEMENTARY MATERIAL

The Supplementary Material for this article can be found online at: https://www.frontiersin.org/articles/10.3389/fchem.2020.536907/full#supplementary-material

## REFERENCES


Andruh, M. (2015). The exceptionally rich coordination chemistry generated by Schiff-base ligands derived from *o*-vanillin. *Dalton Trans.* 44, 16633–16653. doi: 10.1039/C5DT02661J

Feng, D., Zhao, Y., Wang, X., Fang, D., Tang, J., Fan, L., et al. (2019). Two novel metal–organic frameworks based on pyridyl-imidazole-carboxyl multifunctional ligand: selective $CO_2$ capture and multiresponsive luminescence sensor. *Dalton Trans.* 48, 10892–10900. doi: 10.1039/C9DT01430F

Guha, S., and Saha, S. (2010). Fluoride ion sensing by an anion–π interaction. *J. Am. Chem. Soc.* 132, 17674–17677. doi: 10.1021/ja107382x

Guo, Z., Park, S., Yoon, J., and Shin, I. (2014). Recent progress in the development of near-infrared fluorescent probes for bioimaging applications. *Chem. Soc. Rev.* 43, 16–29. doi: 10.1039/C3CS60271K

Guo, Z., Xu, H., Su, S., Cai, J., Dang, S., Xiang, S., et al. (2011). A robust near infrared luminescent ytterbium metal–organic framework for sensing of small molecules. *Chem. Commun.* 47, 5551–5553. doi: 10.1039/c1cc10897b

Hu, J. Y., Ning, Y. Y., Meng, Y. S., Zhang, J., Wu, Z. Y., Gao, S., et al. (2017). Highly near-IR emissive ytterbium(III) complexes with unprecedented quantum yields. *Chem. Sci.* 8, 2702–2709. doi: 10.1039/C6SC05021B

Jankolovits, J., Andolina, C. M., Kampf, J. W., Raymond, K. N., and Pecoraro, V. L. (2011). Assembly of near-infrared luminescent lanthanide host(host-guest) complexes with a metallacrown sandwich motif. *Angew Chem. Int. Ed.* 50, 9660–9664. doi: 10.1002/anie.201103851

Jiang, D., Yang, X., Zheng, X., Bo, L., Zhu, T., Chen, H., et al. (2018). Self-assembly of luminescent 12-metal Zn–Ln planar nanoclusters with sensing properties towards nitro explosives. *J. Mater. Chem. C* 6, 8513–8521. doi: 10.1039/C8TC02426J

Lam, F., Xu, J. X., and Chan, K. S. (1996). Binucleating ligands: synthesis of acyclic achiral and chiral Schiff base-pyridine and Schiff base-phosphine ligands. *J. Org. Chem.* 61, 8414–8418. doi: 10.1021/jo961020f

Li, X., Xu, H., Kong, F., and Wang, R. (2013). A cationic metal–organic framework consisting of nanoscale cages: capture, separation, and luminescent probing of $Cr_2O_7^{2-}$ through a single-crystal to single-crystal process. *Angew Chem. Int. Ed.* 52, 13769–13773. doi: 10.1002/anie.201307650

Liu, C. L., Zhou, L. P., Tripathy, D., and Sun, Q. F. (2017). Self-assembly of stable luminescent lanthanide supramolecular $M_4L_6$ cages with sensing properties toward nitroaromatics. *Chem. Commun.* 53, 2459–2462. doi: 10.1039/C7CC00189D

Liu, G. L., Qin, Y. J., Jing, L., Wei, G. Y., and Li, H. (2013). Two novel MOF-74 analogs exhibiting unique luminescent selectivity. *Chem. Commun.* 49, 1699–1701. doi: 10.1039/C2CC37140E

Liu, X., Yang, X. P., Ma, Y. N., Liu, J. N., Shi, D. L., and Schipper, D. (2020). Construction of a nano-rectangular Zn-Nd complex with near-infrared luminescent response towards metal ions. *Chin. Chem. Lett.* doi: 10.1016/j.cclet.2020.03.016. [Epub ahead of print].

Nagarkar, S., and Desai, A., Ghosh. (2014). A fluorescent metal–organic framework for highly selective detection of nitro explosives in the aqueous phase. *Chem. Commun.* 50, 8915–8918. doi: 10.1039/C4CC03053B

Nagarkar, S. S., Joarder, B., Chaudhari, A. K., Mukherjee, S., and Ghosh, S. K. (2013). Highly selective detection of nitro explosives by a luminescent metal–organic framework. *Angew Chem. Int. Ed.* 52, 2881–2885. doi: 10.1002/anie.201208885

Ning, Y. Y., Tang, J., Liu, Y. W., Jing, J., Sun, Y. S., and Zhang, J. L. (2018). Highly luminescent, biocompatible ytterbium (III) complexes as near-infrared fluorophores for living cell imaging. *Chem. Sci.* 9, 3742–3753. doi: 10.1039/C8SC00259B

Parker, D. (2000). Luminescent lanthanide sensors for pH, $pO_2$ and selected anions. *Coord. Chem. Rev.* 205, 109–130. doi: 10.1016/S0010-8545(00)00241-1

Parker, D., Senanayake, P. K., and Williams, J. G. (1998). Luminescent sensors for pH, $pO_2$, halide and hydroxide ions using phenanthridine as a photosensitiser in macrocyclic europium and terbium complexes. *J. Chem. Soc. Perkin Trans.* 2, 2129–2140. doi: 10.1039/a801270i

Peng, J. B., Zhang, Q. C., Kong, X., Zheng, Y. Z., Ren, Y. P., Long, L. S., et al. (2012). High-nuclearity 3d-4f clusters as enhanced magnetic coolers and molecular magnets. *J. Am. Chem. Soc.* 134, 3314–3317. doi: 10.1021/ja209752z

Qi, X., Jin, Y., Li, N., Wang, Z., Wang, K., and Zhang, Q. (2017). A luminescent heterometallic metal–organic framework for the naked-eye discrimination of nitroaromatic explosives. *Chem. Commun.* 53, 10318–10321. doi: 10.1039/C7CC05345B

Qin, J. H., Ma, B., Liu, X. F., Lu, H. L., Dong, X. Y., Zang, S. Q., et al. (2015). Aqueous- and vapor-phase detection of nitroaromatic explosives by a water-stable fluorescent microporous MOF directed by an ionic liquid. *J. Mater. Chem. A* 3, 12690–12697. doi: 10.1039/C5TA00322A

Sedaghat, S., Jeong, S., Zareei, A., Peana, S., Glassmaker, N., and Rahimi, R. (2019). Development of a nickel oxide/oxyhydroxide-modified printed carbon electrode as an all solid-state sensor for potentiometric phosphate detection. *New J. Chem.* 43, 18619–18628. doi: 10.1039/C9NJ04502C

Sheldrick, G. H. (1997). *SHELX 97, A Software Package for the Solution and Refinement of X-Ray Data*. Göttingen: University of Göttingen.

Shi, D. L., Yang, X. P., Chen, H. F., Jiang, D. M., Liu, J. N., Ma, Y. N., et al. (2019). Large $Ln_{42}$ coordination nanorings: NIR luminescence sensing of metal ions and nitro explosives. *Chem. Commun.* 55, 13116–13119. doi: 10.1039/C9CC07430A

Shi, P. F., Hu, H. C., Zhang, Z. Y., Xiong, G., and Zhao, B. (2015). Heterometal–organic frameworks as highly sensitive and highly selective luminescent probes to detect $I^-$ ions in aqueous solution. *Chem. Commun.* 51, 3985–3988. doi: 10.1039/C4CC09081K

Sun, X., Wang, Y., and Lei, Y. (2015). Fluorescence based explosive detection: from mechanisms to sensory materials. *Chem. Soc. Rev.* 44, 8019–8061. doi: 10.1039/C5CS00496A

Wang, B., Zang, Z., Wang, H., Dou, W., Tang, X., Liu, W., et al. (2013). Multiple lanthanide helicate clusters and the effects of anions on their configuration. *Angew Chem. Int. Ed.* 52, 3756–3759. doi: 10.1002/anie.201210172

Wen, Q., Tang, Y., Li, K., and Zheng, Y. (2019). Structural and optical features of lanthanide species-derived functional hydrogel. *Soft Mater.* 17, 350–358. doi: 10.1080/1539445X.2019.1606013

Xiao, Y., Cui, Y., Zheng, Q., Xiang, S., Qian, G., and Chen, B. (2010). A microporous luminescent metal–organic framework for highly selective and sensitive sensing of $Cu^{2+}$ in aqueous solution. *Chem. Commun.* 46, 5503–5505. doi: 10.1039/c0cc00148a

Xie, R., Tu, M. B., and Elder, T. (2016). Substituent effect of phenolic aldehyde inhibition on alcoholic fermentation by saccharomyces cerevisiae. *Energy Fuels* 30, 3078–3084. doi: 10.1021/acs.energyfuels.5b03034

Xu, H. B., Wen, H. M., Chen, Z. H., Li, J., Shi, L. X., and Chen, Z. N. (2010). Square structures and photophysical properties of $Zn_2Ln_2$ complexes (Ln = Nd, Eu, Sm, Er, Yb), *Dalton Trans.* 39, 1948–1953. doi: 10.1039/B919170D

Yang, J., Dai, Y., Zhu, X., Wang, Z., Li, Y., Zhuang, Q., et al. (2015). Metal–organic frameworks with inherent recognition sites for selective phosphate sensing through their coordination-induced fluorescence enhancement effect. *J. Mater. Chem. A* 3, 7445–7452. doi: 10.1039/C5TA00077G

Yang, X. P., Jones, R. A., and Huang, S. M. (2014). Luminescent 4f and d-4f polynuclear complexes and coordination polymers with flexible salen-type ligands. *Coord. Chem. Rev.* 273, 63–75. doi: 10.1016/j.ccr.2013.11.012

Yuan, L., Lin, W., Zheng, K., He, L., and Huang, W. (2013). Far-red to near infrared analyte-responsive fluorescent probes based on organic fluorophore platforms for fluorescence imaging. *Chem. Soc. Rev.* 42, 622–661. doi: 10.1039/C2CS35313J


**Conflict of Interest:** The authors declare that the research was conducted in the absence of any commercial or financial relationships that could be construed as a potential conflict of interest.